

University of Groningen

High Resolution Imaging of Chalcogenide Superlattices for Data Storage Applications

Kooi, Bart J.; Momand, Jamo

Published in:
Physica Status Solidi - Rapid Research Letters

DOI:
[10.1002/pssr.201800562](https://doi.org/10.1002/pssr.201800562)

IMPORTANT NOTE: You are advised to consult the publisher's version (publisher's PDF) if you wish to cite from it. Please check the document version below.

Document Version
Publisher's PDF, also known as Version of record

Publication date:
2019

[Link to publication in University of Groningen/UMCG research database](#)

Citation for published version (APA):
Kooi, B. J., & Momand, J. (2019). High Resolution Imaging of Chalcogenide Superlattices for Data Storage Applications: Progress and Prospects. *Physica Status Solidi - Rapid Research Letters*, 13(4), [1800562].
<https://doi.org/10.1002/pssr.201800562>

Copyright

Other than for strictly personal use, it is not permitted to download or to forward/distribute the text or part of it without the consent of the author(s) and/or copyright holder(s), unless the work is under an open content license (like Creative Commons).

The publication may also be distributed here under the terms of Article 25fa of the Dutch Copyright Act, indicated by the "Taverne" license. More information can be found on the University of Groningen website: <https://www.rug.nl/library/open-access/self-archiving-pure/taverne-amendment>.

Take-down policy

If you believe that this document breaches copyright please contact us providing details, and we will remove access to the work immediately and investigate your claim.

Downloaded from the University of Groningen/UMCG research database (Pure): <http://www.rug.nl/research/portal>. For technical reasons the number of authors shown on this cover page is limited to 10 maximum.

High Resolution Imaging of Chalcogenide Superlattices for Data Storage Applications: Progress and Prospects


Bart J. Kooi* and Jamo Momand

Phase-change materials (PCMs) based on Ge–Sb–Te alloys are a strong contender for next-generation memory technology. Recently, PCMs in the form of GeTe–Sb₂Te₃ superlattices (CSLs) have shown superior performance compared to ordinary PCM memory, which relies on switching between amorphous and crystalline phases. Although detailed atomic structure switching models have been developed with the help of ab-initio simulations, there is still fierce scientific debate concerning the experimental verification of the actual crystal structures pertaining to the two CSL memory states. One of the strongest techniques to provide this information is (scanning) transmission electron microscopy ((S)TEM). The present article reviews the analyses of CSLs using TEM-based techniques published during the last seven years since the seminal 2011 Nature Nanotechnology paper of Simpson et al., showing the superior performance of the CSL memory. It is critically reviewed what relevant information can be extracted from the (S)TEM results, also showing the impressive progress that has been achieved in a relatively short time frame. Finally, an outlook is given including several open questions. Although debate on actual switching mechanism in CSL memory is clearly not settled, still there is consensus in this field that CSL research has a bright future.

1. Introduction

In the modern age of big data, internet of things and cloud computing the demand for memory and storage technology is rapidly increasing. At the same time, Moore's law is approaching the limits of the currently market-dominant DRAM and Flash, necessitating new types of memory devices or computing paradigms altogether.^[1,2] One of the contenders for such memory technologies exploits phase-change materials (PCM), which are typically based on ternary Ge–Sb–Te (GST) alloys.^[3,4] These materials have a large optical and electrical contrast between their crystalline and amorphous phases, combined with fast switching, thermal stability and scalability, making them highly suitable for fast non-volatile memory applications.

Prof. B. J. Kooi, Dr. J. Momand
Zernike Institute for Advanced Materials
Nijenborgh 4, 9747AG Groningen, The Netherlands
E-mail: b.j.kooi@rug.nl

 The ORCID identification number(s) for the author(s) of this article can be found under <https://doi.org/10.1002/pssr.201800562>.

DOI: 10.1002/pssr.201800562

PCM technology has already been successfully implemented in rewritable optical disks such as CD, DVD and Blu-Ray, and is currently under investigation for electronic^[5] and photonic memory,^[6,7] optical display^[8,9] and neuromorphic applications.^[10,11]

One of the big problems of PCM, however, is the large programming current (I_{prog}) it requires to switch the memory devices from the crystalline state (SET) to the amorphous state (RESET). Due to Joule heating this I_{prog} is coupled to the SET resistance (R_{set}) with the approximate relation of $I_{\text{prog}} \times R_{\text{set}} = 1$, where the energy usage of the devices is balanced against the latency of the SET state for applications.^[12] Recently the field has undergone new developments to go beyond this Joule heating limitation using, e.g., confined dimensionality,^[13,14] carbon nanotube electrodes,^[15] but also by using GeTe/Sb₂Te₃ chalcogenide superlattices (CSL).^[16–18] The latter memory devices showed an improved performance compared with mixed GST alloys, in terms of programming current, switching speed and possibly magnetic functionality.^[19,20] Most importantly, they switched at lower I_{prog} at approximately the same R_{set} , going beyond the Joule heating constraint. This has been attributed to a new phase-change mechanism in PCM and created a lot of excitement in the field of PCM.

Since this superior memory performance was observed in CSL-based devices, worldwide research on CSL has been drastically intensified. Although in the seminal paper of Simpson et al. the actual switching mechanism underlying the memory performance was not explained, it was already concluded, also based on support by transmission electron microscopy (TEM) observations, that the switching occurred fully in the crystalline state.^[16] This is highly remarkable, because in traditional PCMs (based on very similar materials on the GeTe–Sb₂Te₃ tie-line in the GST ternary phase diagram) the two memory states are directly linked to crystalline and amorphous phases, where switching from the former to the latter generally proceeds via melt-quenching. Therefore, it is a logical step to attribute the superior performance of the CSL based memory to a switching mechanism between two crystalline states avoiding the melt-quench step and thereby avoiding a step that is energy intensive and facilitates sample degradation.

The amorphous-crystalline transition in PCMs is accompanied by a profound change in electronic structure, which is investigated and debated up to this day.^[21–23] One of the early insights was provided through extended X-ray absorption fine structure (EXAFS) studies of the crystallization of GST by Kolobov et al.^[24] In that work the authors showed that, while the Te sublattice was mostly intact, a significant part of the Ge atoms had a different coordination in the amorphous and crystalline states, i.e. tetrahedral and octahedral positions, respectively. From these results, the idea of the Ge umbrella-flip mechanism was born, see **Figure 1a**. Because of this model some of the authors suggested that localizing Ge atoms in a superlattice would result in a more efficient umbrella flip-transition, see **Figure 1b**.^[25] After these ideas and insights, such superlattices were grown and tested experimentally, resulting in the renowned Nature Nanotechnology publication of Simpson et al. in 2011.^[16]

The interest to better understand the actual switching behavior in the CSL calls upon a technique that can directly provide information on the crystal structure details. One of the most powerful techniques to do this is TEM. Still, conventional TEM is based on coherent interference of waves and suffers from spatial delocalization. This makes it difficult to directly interpret the structure, because atomic columns cannot be directly coupled to dark or bright spot intensities in the image. Fortunately, the last decade also incoherent scanning TEM (STEM) has become a widespread technique. When STEM imaging occurs with electrons scattered by the sample to high angles, the interpretation becomes much more straightforward. Then the imaging becomes directly related to how the average atomic number Z (typically $\approx Z^2$) varies spatially over the sample.^[26] When the electron probe in the STEM can be made smaller than the distance between atomic columns, then atomic scale Z -contrast imaging is possible with high-angle annular dark field (HAADF) STEM. The introduction of field emission guns in the nineties and application of aberration (probe) correctors in the first decade of this century made this development of atomic scale Z -contrast imaging possible and have thus strongly contributed to the current popularity of this technique.

The aim of the present article is to review such important TEM and STEM results obtained on CSL in papers published since the seminal 2011 Nature Nanotechnology paper of Simpson et al.,^[16] where we treat the papers mostly in chronological order. Later we will also pay attention to specific topics such as intermixing between GeTe and Sb₂Te₃ that arose from this research. We try to summarize what can be learned from these results in relation to the memory switching mechanism and we will finally give an outlook on possible next steps in the research of CSL with TEM-based techniques.

2. Results and Discussion

2.1. Interfacial Phase Change Memory and the Quest for Ge–Ge Bonds

Figure 2 shows most of the important TEM results presented in the 2011 Nature Nanotechnology paper of Simpson et al.,^[16] where **Figure 2a** shows a cross-section HRTEM image of a CSL



Prof. Bart J. Kooi obtained his PhD degree in materials science in 1995 from Delft University of Technology, Netherlands. Since then, he worked at the University of Groningen (Netherlands) as assistant, associate and full professor, starting in 2009 his own research group Nanostructured Materials and Interfaces within the Zernike

Institute for Advanced Materials. He published over 180 papers in peer-reviewed international scientific journals. His main research interests are nanostructure–property relations, interfaces, phase transformations, transmission electron microscopy and telluride and antimonide based materials.



Dr. Jamo Momand obtained his BSc in Applied Physics in 2012 and his MSc in the Top Master Programme in Nanoscience in 2014 from the University of Groningen, The Netherlands. He specialized in the field of superlattice phase-change materials within the PASTRY project consortium in the group of Prof. Bart J. Kooi at the Zernike Institute

for Advanced Materials at the University of Groningen, where he obtained his PhD degree in 2017. He is currently specializing in aberration corrected TEM/STEM for investigating nanomaterials related to electronics applications.

film. The crystal planes parallel to the substrate surface are clearly resolved, indicating that the film is highly textured. However, due to the limited resolution and the contrast mechanism of conventional TEM it is not possible to identify individual GeTe and/or Sb₂Te₃ sublayers. Also, the authors claim that they grow structures with two GeTe bilayers, but write that the GeTe sublayer has a thickness of 1 nm. This is not consistent, because three (and not two) GeTe bilayers have a thickness very close to 1 nm, and the number of bilayers can definitely not be verified based on these TEM results.

Figure 2b shows a cross-section image of an actual CSL memory device. Moreover, the authors state that the image is taken from a device in the RESET (high resistance) state. For a traditional PCM cell this would mean that an amorphous dome should be visible, which is not the case here. Although the resolution in the image is limited, the active region appears fully crystalline and for most part highly textured. In contrast, the authors also deliberately RESET a similar cell with the same high-power pulse conditions as used for a traditional GST PCM and then, as can be seen in **Figure 2c**, clearly an amorphous dome (derived from melt-quenching) is formed above the TiN heater.

These results indicate convincingly that switching in the CSL occurs differently from the familiar melt-quench step of mixed

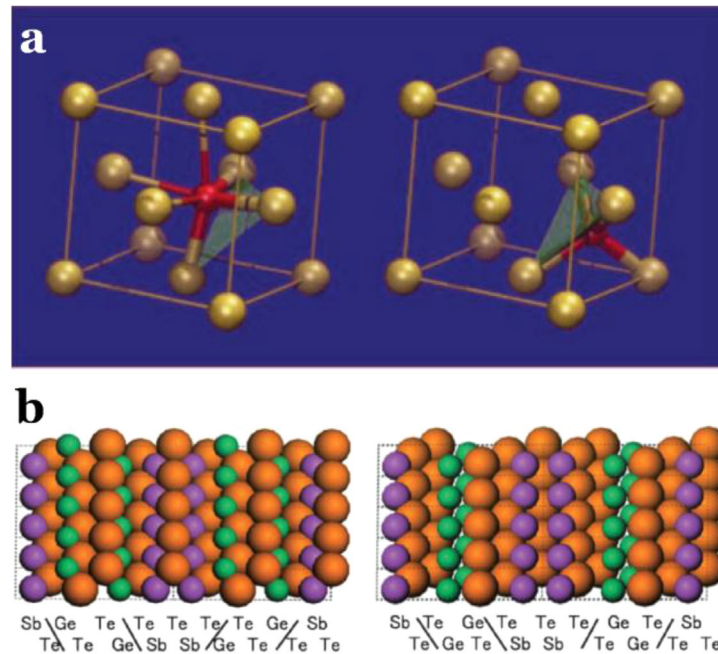


Figure 1. a) Umbrella flip model for the structural transition in GST. The left image shows Ge (red) in the octahedral position and the right in the tetrahedral position of the Te (yellow) sublattice. Reproduced with permission.^[24] Copyright 2004, Nature Publishing Group. b) Proposed superlattice structure of GeTe–Sb₂Te₃ to confine the Ge umbrella flip. Reproduced with permission.^[25] Copyright 2008, The Japan Society of Applied Physics.

GST. However, two points of caution have to be added here. First, the conventional TEM imaging mode relies on interference of waves which can cause significant delocalization of information in-between GeTe and Sb₂Te₃ interfaces or due to disorder. Although the results prove that an amorphous dome is not present, it cannot be fully ruled out that one of the thin sublayers is amorphous and the other still crystalline. Secondly, it is possible that crystallization of one of the sub-layer types occurred during the TEM sample preparation, which likely involved ion-

milling like in a focussed ion beam (FIB) system. This does not occur for the amorphous dome of Figure 2c, however, for very thin amorphous sublayers (of one type) in-between crystalline sublayers (of the other type) it cannot be ruled out that crystallization occurs during the TEM sample preparation.

The TEM results shown in Figure 2 are strong, but still miss important information. They particularly lack data on experimental atomic stacking required for ab-initio calculations to model the switching, like suggested to occur via a collective

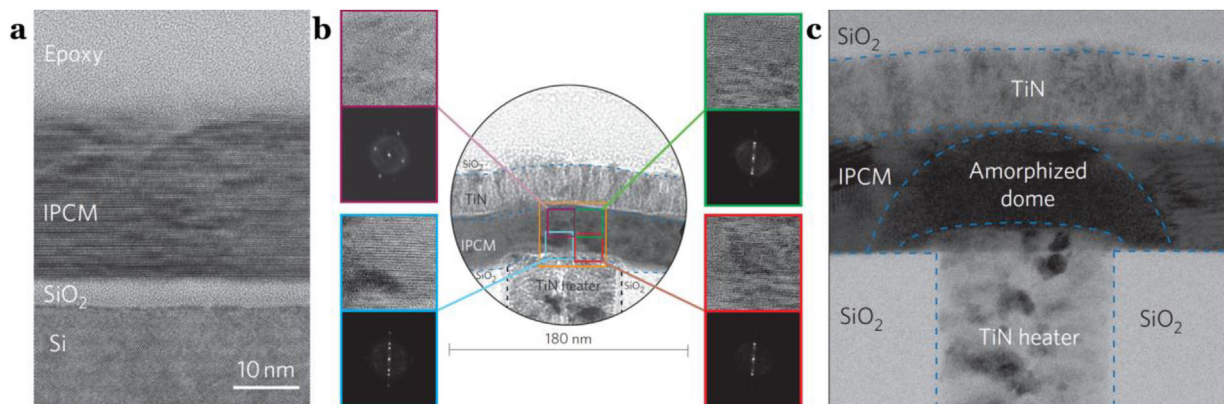


Figure 2. a) High-resolution TEM image of a typical GeTe–Sb₂Te₃ CSL film, as grown by sputtering on silicon. The GeTe layers are indicated to be 1 nm thick, and the Sb₂Te₃ layers 4 nm thick. b) Central circular image: TEM image of a GeTe–Sb₂Te₃ CSL structure in the RESET state after 1000 SET–RESET cycles. In contrast to GST, the TEM image shows that there is no amorphous region surrounding the TiN heating electrode. Side panels: High-resolution TEM images (top) and corresponding selected area electron diffraction patterns (bottom) for the four regions inside the colored squares in the central image. The layered CSL structure and associated diffraction spots are readily visible in all images. c) A CSL device that was deliberately RESET with the same high-power pulse conditions required by GST. As with GST, an amorphized dome is formed above the TiN heater, resulting in destruction of the superlattice structure and irreversible damage to the CSL device. Reproduced/adapted with permission.^[16] Copyright 2011, Nature Publishing Group.

“umbrella flip” of Ge atoms at the interface between GeTe and Sb_2Te_3 .^[27] The best tool to provide such information directly is HAADF-STEM, where Ge due to its lower Z number can be distinguished well with respect to Sb and Te. This route was indeed followed by the group of Tominaga and the first HAADF-STEM results were shown in 2014, see **Figure 3**.^[28] The images show good atomic resolution, which has been used to overlay atomic models. However, the major problem now is that the overlaid atomic models do not agree with the intensities in the Z-contrast images. For instance, the lightest element Ge must be distinctly coupled to the lowest intensity bright dots. Since quantitative analysis of the intensities of the Z-contrast images readily shows that there is no such correlation concerning the type of elements present, the overlaid models cannot be taken seriously. The second problem is that such small fields of view make it difficult to judge whether the provided images are representative for the RESET and SET states. Large overview images and many images with sufficient resolution from this overview could help, but it would also be preferred to have a technique which averages the sample/film over a large volume like X-ray diffraction. The same two problems (i.e. uncorrelated intensities and too small imaged areas) hold for the HAADF-STEM results with the overlaid models shown in a 2015 paper by Tominaga et al.^[29]

In 2014 Saito et al. published a paper on $\text{SiTe-Sb}_2\text{Te}_3$ superlattices with nice TEM results, containing both large overview bright-field TEM and atomic resolution HAADF-STEM, see **Figure 4a–c**.^[30] Contrast between the SiTe and Sb_2Te_3 sublayers is good in both images due to the much lower Z of Si compared to Sb and Te (where Si is even clearly lower than Ge). The overview image shows the flatness of the Si substrate on which the CSL is grown, nice periodic repetitions in the CSL and the smooth CSL surface. Now in the HAADF-STEM image (Figure 4c) two SiTe sublayers can be distinguished well, because as expected they have lower intensities than Sb and Te. Despite the nice planar nature of the sublayers in the CSL parallel to the substrate surface, as seen in the overview image (Figure 4a and 4b), still the HAADF-STEM image (Figure 4c) shows that the Si-rich sublayers are not aligned well with the crystal planes. This makes exact pinpointing of the Si atomic layers hard. For the thin SiTe sublayer at the top in the image the crystal plane sequence

seems to be Si–Te–Si–Te and not Te–Si–Si–Te as shown in the overlaid model. But now we cannot sufficiently zoom in to distinguish the actual structure clearly.

Thus far good experimental evidence of a chalcogenide structure with neighboring Ge atomic planes has been lacking. Until in 2017 a publication on $\text{Ge}_4\text{Se}_3\text{Te}$ demonstrated beautifully by STEM analysis (see **Figure 5**) that Ge–Ge planes become directly bonded, but that this bond disappears when the Se is replaced by Te and we move back to GeTe.^[31] In Figure 5a the overlaid atomic model is in excellent agreement with the HAADF-STEM image (Figure 5a) and although there is no doubt about the atomic structure there is even further support from the energy dispersive X-ray spectroscopy (EDX) map (Figure 5b). Such quality of experimental evidence is required to prove the existence of Ge–Ge bonds within CSL.

High quality atomic resolution HAADF-STEM images were also published in 2014 by Takaura et al. where their work strongly focused on different types of Ge-Te atomic plane sequences for explaining the switching behavior of the CSL memory.^[32] An example image with coupled atomic model is shown in **Figure 6**. In the image the Te planes corresponding to the ones with the brightest spots can be distinguished well. The red box centers on a defect where a van-der-Waals (vdW) gap jumps two atomic layers down when following the gap from left to right. As expected, the Te planes are directly adjacent to the vdW gap. Away from the vdW gap, again as expected, Ge and Sb crystal planes are present in-between the Te planes. However, if the film contained pure Ge or Sb atomic planes, the difference between Ge and Sb should be readily visible in the HAADF-STEM image. This is not the case, because all these crystal planes in-between Te planes have more or less similar brightness. The only solution to explain this discrepancy is that pure Ge and Sb planes do not exist, but are mixed. In the model below the image the atomic sequence is taken as $\text{vdWgap-Te-Ge-Te-Sb-Te}$, but the image definitely does not allow this distinction between Ge and Sb planes. Mixing of Ge and Sb on one sublattice and Te on another sublattice is well-known to the PCM community since the work of Yamada et al.^[33] They showed that the standard switching in GST occurs between the amorphous phase and a meta-stable rocksalt structure with Te on one fcc sublattice (4(a) sites) and Ge, Sb and vacancies (25% for GST124, 20% for GST225) mixed on the other

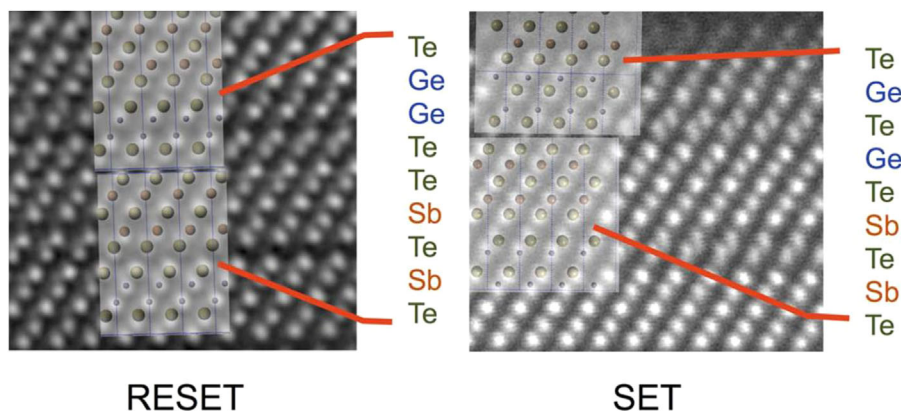


Figure 3. HAADF-STEM images of two different crystalline phases (RESET and SET) of a $\text{GeTe-Sb}_2\text{Te}_3$ CSL with superimposed simulation models. Reproduced with permission.^[28] Copyright 2014, Nature Publishing Group.

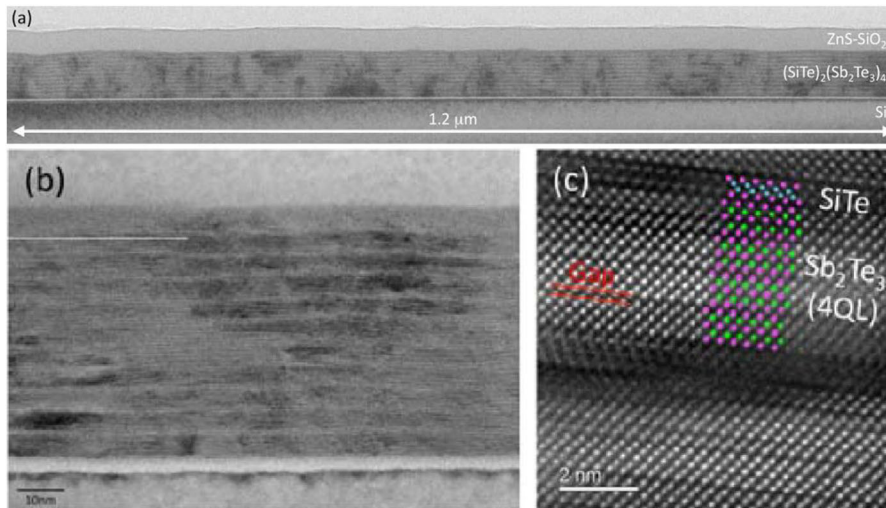


Figure 4. a and b) TEM cross-sectional image of a ten-period SiTe–Sb₂Te₃ CSL as deposited by sputtering at 553 K. c) HAADF-STEM image of “(SiTe)₂–(Sb₂Te₃)₄” CSL. Reproduced with permission.^[30] Copyright 2014, Wiley-VCH.

interpenetrating fcc sublattice (4(b) sites). In order to produce sufficiently crystalline quality CSL, growth temperatures are generally in the range 200–250 °C and therefore it is expected that also in CSL the atomic planes of Ge and Sb do not stay pure, but can show some degree of intermixing at these relatively high temperatures. Next to this intermixing apparently also defects like shown in the red box, which are called bilayer defects, can be present in CSL. These effects of mixing and defects will be discussed in more detail in the next sections and they make interpretation of the structure in CSL less straightforward and also

explain why the interpretation of the intensities in the images like shown in Figure 3 has been problematic.

2.2. GST Formation and Intermixing

Until 2015 there was a dominant belief in a switching mechanism where Ge atomic planes at the interface between GeTe and Sb₂Te₃ would show a kind of collective umbrella flip, with only debate about the details of such flip.^[28,27,29,34–36,32,37–39] Then a paper was

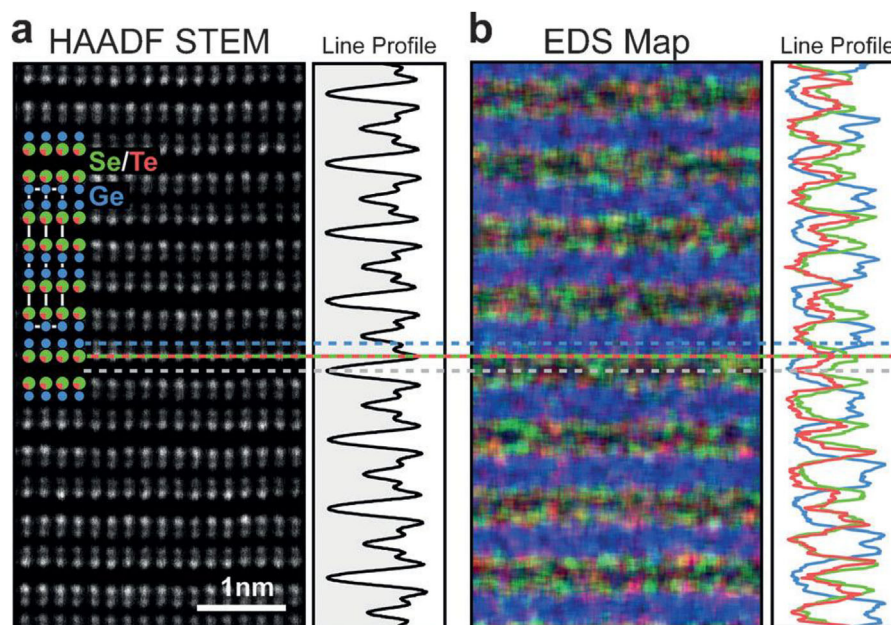


Figure 5. a) HAADF-STEM image of Ge₄Se₃Te viewed along the [110] zone axis and its corresponding line profile (intensity integrated along the horizontal axis). The atomic positions in this zone axis are also shown. Ge blue, Se green, Te red. b) EDX map and corresponding line profiles. Dashed horizontal lines indicate the positions of different layers across both panels. Reproduced with permission.^[31] Copyright 2017, Wiley-VCH.

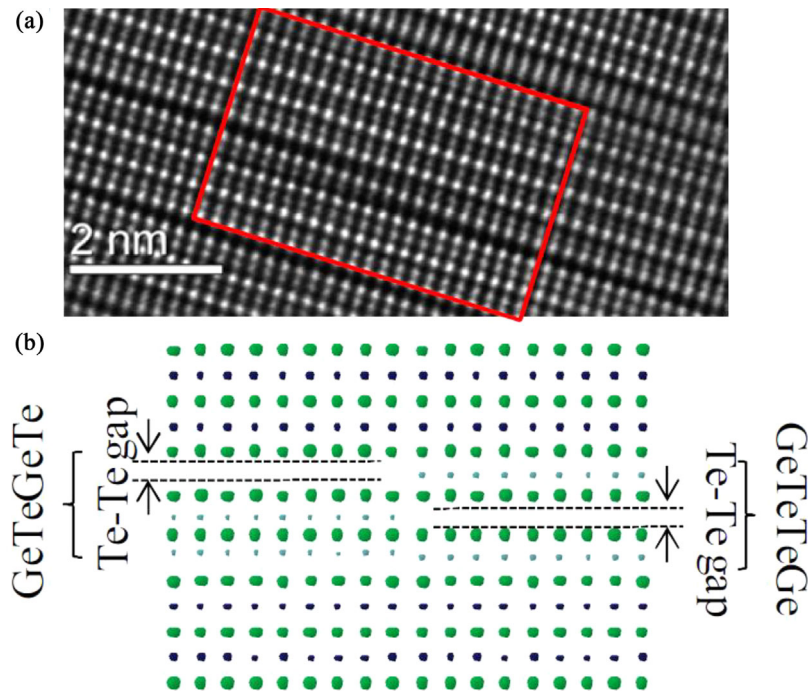


Figure 6. Upper panel: HAADF-STEM image of GeTe-Sb₂Te₃ CSL showing a so-called bilayer defect that allows a shift of the vdW gaps 2 atomic layers up or down. Lower panel: Atomic model derived from the image in the upper model. Note however, that the distinction between Ge atomic columns (small green dots in the model) and the Sb atomic columns (blue dots in the model) made in the atomic model does not agree with the Z-contrast that is present in the image. This Z contrast proves that strong intermixing of Ge and Sb must have occurred. Reproduced with permission.^[32] Copyright 2017, IEEE.

published directly showing that GeTe-Sb₂Te₃ superlattices reconfigure into alternating GST and Sb₂Te₃ when grown at a usual temperature of 230 °C and completely reconfigure into the stable (trigonal) crystal structure of GST when annealed at 400 °C.^[40] **Figure 7** shows example HAADF-STEM images from this paper demonstrating that the GST grown at 230 °C can range from GST124 (short for GeSb₂Te₄, and similar for others) to GST427, where the line scan below each image taken over the central vdW block in each image shows the tendency that Ge is present in the center of each block and Sb more towards the vdW gaps. This tendency and the structures of the stable trigonal crystal structure of GST have already been demonstrated by Matsunaga et al. in 2004^[41–43] and refined by for instance Urban et al. in 2013.^[44]

So, the actual structure of stable GST does not imply that Ge and Sb are randomly mixed on the “cation” sublattice in-between the Te “anion” sublattice, because an Sb-rich plane is directly following the Te plane adjacent to the vdW gap and Ge-rich plane(s) are more distant from the vdW gap. The implication of this reconfiguration of GeTe-Sb₂Te₃ into GST-Sb₂Te₃ for the potential switching mechanism in the CSL memory is considerable, because it makes the collective umbrella flip of Ge atoms near the vdW gaps rather unlikely in these structures.

It is obvious that each GeTe sublayer, when reconfiguring into a GST sublayer bounded by vdW gaps, consumes one Sb₂Te₃ quintuple layer. When the GeTe sublayer consists of two bilayers then a GST225 sublayer is formed, when it consists of three bilayers GST326 is formed, etc. The atomic scale mechanism by which this process occurs during growth has been put forward by Wang et al.^[45] When a GeTe bilayer is deposited onto Sb₂Te₃ the

uppermost Sb layer and the newly added Ge layers will exchange (by diffusional jumps), i.e., Sb moves upwards and Ge downwards. This process repeats when the next GeTe bilayer is added. Depending on the local number of GeTe bilayers deposited all possible Ge_xSb₂Te_{3+x} can be formed as observed experimentally (see Figure 7). This mechanism also in a natural manner explains why after growth the Sb layer at the top of a GST vdW layer is clearly intermixed with Ge and why hardly any intermixing occurs for the Sb layer at the bottom of the GST layer. This difference between top and bottom Sb layers is also well-observable in Figure 7 both in the images and the line scans.

The GeTe-Sb₂Te₃ superlattices in Refs. ^[40] and ^[45] were grown using molecular beam epitaxy (MBE), which in principle allows more accurate control than sputtering that was used in all earlier work on these superlattices. Therefore, a potential criticism can be that the GeTe-Sb₂Te₃ CSL reconfigure into GST-Sb₂Te₃ during the slow growth process of MBE, but not during sputtering. However, a follow-up work showed that this reconfiguration was also observed for sputtered films.^[46] Therefore, it seems that this reconfiguration is showing the underlying thermodynamic tendency irrespective of the actual growth technique, but it is only dependent on temperature and time available during growth. Later research on GeTe-Sb₂Te₃ superlattices grown by pulsed-laser deposition^[47] and by magnetron sputtering^[48] indeed confirmed that this GST formation is generally observed. A figure from this last reference containing HAADF-STEM images is reproduced here in **Figure 8**, showing in the top image that the central vdW layer containing nine planes can be typified as GST225, but the bottom figure contains a 19 atomic planes thick GST layer showing a concentration profile for the Ge and Sb on the cation sublattice

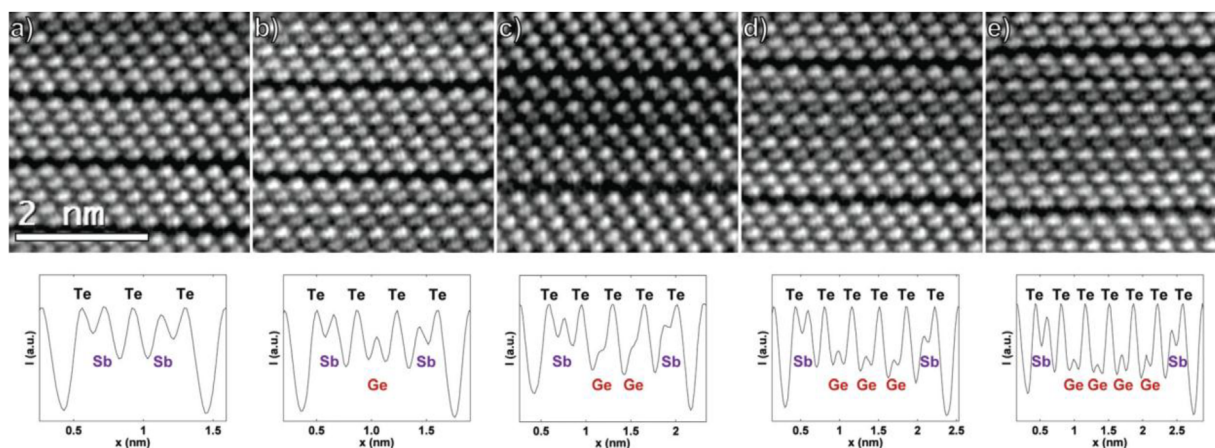


Figure 7. Variety of vdW layers formed in GeTe-Sb₂Te₃ CSL as grown by MBE at 230 °C with the aim to grown 1 nm GeTe and 3 nm Sb₂Te₃ sublayers. The intensity line scans corresponding to the HAADF-STEM micrographs cover larger regions than shown in the representative images and they are taken in the images from bottom to top. 5-layer (a), 7-layer (b), 9-layer (c), 11-layer (d), and 13-layer (e) vdW structures. In the line scans the low intensity dips correspond to vdW gaps and the peaks to the Ge, Sb, and Te atomic planes. The Z-contrast in the image allows relatively straightforward identification of Ge, Sb, and Te planes. Note that several atomic planes already show evidence of Ge/Sb intermixing. Reproduced under the terms of a Creative Commons Attribution-NonCommercial 3.0 Unported Licence.^[40] Copyright 2015, The Royal Society of Chemistry.

with probably nearly pure Ge in the central four layers and increasingly Sb-rich layers towards the vdW gaps. The vdW gap on the top of the GST layer in Figure 8b is very distinct, but the one at the bottom is not. It seems that the bottom two atomic planes of the GST layer have kind of half vdW gaps on top and at the bottom. The probable explanation for this observation is that these two planes are part of a bilayer defect as we have seen for the first time in this manuscript in Figure 6 and as will be treated in more detail in the next section.

2.3. Bilayer Defects

The bilayer defects observed in Figure 6 and probably in Figure 8b are not unique for CSL, but are generally observed in layered GST compounds (approaching the stable GST structure) as for instance obtained during epitaxial growth.^[49] Another example of the observation of bilayer defects as imaged by HAADF-STEM is shown in Figure 9a and b.^[50] These defects are always directly adjacent vdW gaps and the predominant reason for their existence appears to be that they can shift vdW gaps two layers up or down. From the Z-contrast analysis it is clear that the bilayer defect always involves a Te plane and an Sb-rich plane and not a Te-plane and a Ge-rich plane. It has recently been shown that this conclusion is probably correct, based on atomic resolution STEM where EDX is used instead of HAADF;^[51] see an example image from this work in Figure 10. Using EDX the distinction between Sb and Te (and of course also Ge) can in principle be made directly (when signal to noise ratio is sufficient), whereas in HAADF images Te and Sb cannot be distinguished. Still, in HAADF the signals (intensities) can be measured to date more precisely as the signals in EDX which are currently still quite noisy (see Figure 10). Moreover, since only the Sb planes are a bit intermixed with Ge and not the Te planes, still the distinction between the Te and Sb-rich planes can be made based on HAADF images, because the Sb-rich planes

correspond to (slightly) lower intensity in these images (see also Figure 6).

Actually, the bilayer defect always has a limited width, because on both sides the stacking appears at first sight perfect. However, one can also argue that the bilayer defect marks a transition from a properly stacked region to a stacking faulted region.^[47,49,52] The width of this transition varies, where a likely origin for this variation is that we image the bilayer defects in different projection directions. So in fact, the bilayer defects have more line character, where the line separates the different types of stacking on both sides. A line defect is typically associated with a dislocation, where a *partial* dislocation separates a normal stacked region with a stacking-faulted region. So, the present bilayer defect seems to have a strong analogy with a partial dislocation. However, as will be explained below the bilayer defect cannot be associated with a dislocation (or disclination), because it is more involved than only a translation (or rotation).

Ref.^[49] showed that an array of such defects in a GST film was located in a correlated manner with respect to a substrate surface step. Then it is relatively obvious that they can account for stacking differences as for instance induced by the step. The STEM images in Figure 9 hold for a GeTe-Sb₂Te₃ CSL annealed for 1 h at 300 °C (after it was grown at 230 °C). Bilayer defects were clearly more abundant in the 300 °C annealed sample than in the as-deposited (230 °C) sample or the 400 °C annealed sample. These defects were not correlated with substrate surface steps. Interestingly, these defects are probably correlated with the transformation from the initial as-deposited CSL composed of alternating GST and Sb₂Te₃ into the stable (trigonal) crystal structure of GST.

In order to have better statistical data on this transformation relatively large overview HAADF-STEM images still containing sufficient atomic resolution were analyzed in an automated fashion to extract the different types of vdW blocks present in the images.^[50] The type of vdW block is classified based on the number of atomic layers (of any type) present in-between

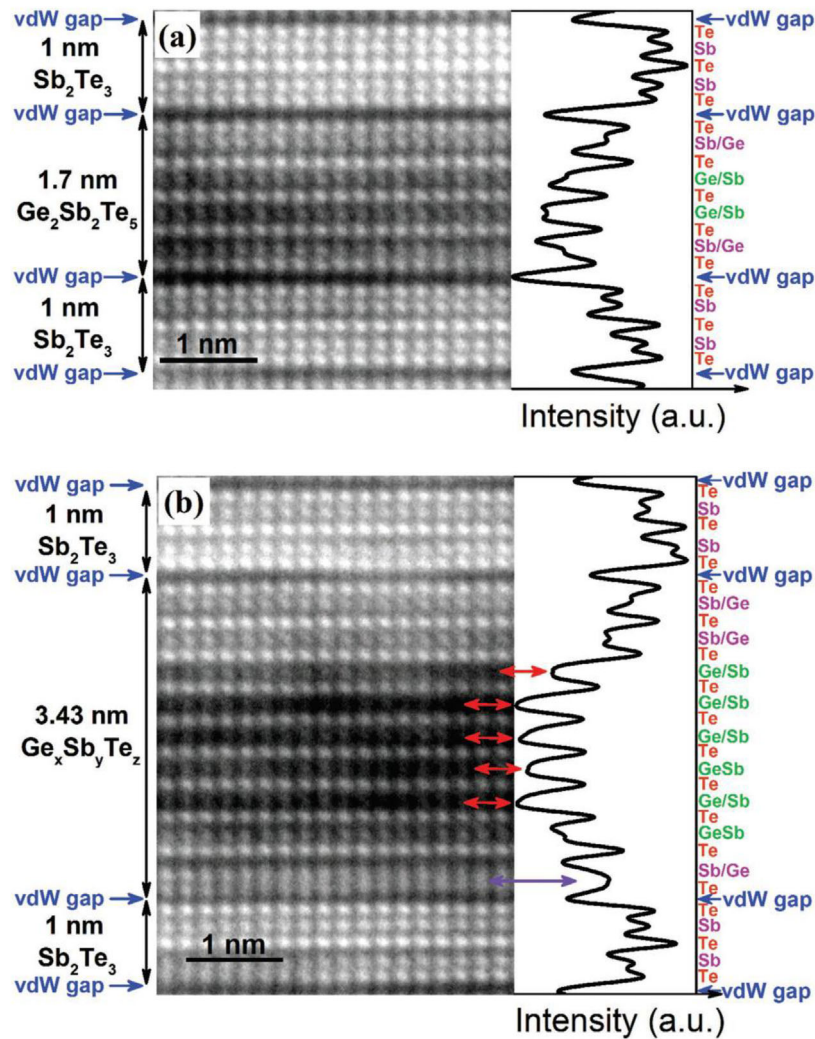


Figure 8. HAADF-STEM images of an optimized $[(\text{GeTe})_2/(\text{Sb}_2\text{Te}_3)_4]_{24}$ CSL deposited by co-sputtering with an Te target. Viewing direction is $[210]$. The images in (a) and (b) illustrate two different types of stacking present in the CSL. Curves on the right of each image are vertical linescans integrated over the image width. vdW gaps are indicated with blue arrows. Atomic columns containing heavy atoms (Te or Sb) appear significantly brighter than those containing Ge atoms due to the Z-contrast in the HAADF mode. a) Two Sb_2Te_3 QLs and one GST225 block (nine planes) separated by vdW gaps are identified. b) Two Sb_2Te_3 QLs and an unusual 19 plane stacking are visible. The latter contains dark zones, pointed out by double red arrows, which do not correspond to vdW gaps (see text). Planes containing Ge and Sb atoms are denoted as Ge/Sb for Ge-rich planes and Sb/Ge for Sb-rich planes. Reproduced with permission.^[48] Copyright 2018, Wiley-VCH.

successive vdW gaps or vacancy layers. For instance a 5-layer block will be an Sb_2Te_3 quintuple with thickness of 1 nm, a 7-layer stack is probably GST124, a 9-layer block GST225, etc. The areal fraction of these different types in the recorded images is plotted in Figure 9c for the different annealing conditions. The analysis demonstrates that in principle only odd-numbered blocks are present. In the as-deposited film a wide distribution is present ranging from 5 layers to 17 layers with local maxima for 5 and 11 layers. Since the nominal GeTe thickness grown is 1 nm, which corresponds to 3 GeTe bilayers, it is expected that when this GeTe sublayer reacts with (is passivated by) one Sb_2Te_3 quintuple an 11 layered GST326 block is formed. When deposition conditions are ideal and when this reaction proceeds perfectly then only 5 and 11 layered blocks should be present in the reconfigured CSL. Although this preference for films to contain

5 and 11-layered blocks is clearly observable, still a relatively wide distribution of vdW blocks is present. Interestingly, after annealing at higher temperatures (300 and 400 °C) this distribution is narrowing down and after 1 h at 400 °C only 7 and 9-layered blocks are present. This implies that effectively all Sb_2Te_3 quintuples have reacted with the 11 to 17 layered GST to form 7 and 9 layered GST. This process clearly demonstrates that the reconfiguration of $\text{GeTe-Sb}_2\text{Te}_3$ into GST is thermodynamically favored.

It is possible that this reconfiguration into GST fully occurs by atomic diffusion. Indeed this is expected to hold for 400 °C annealing. However, at lower temperatures like 300 °C atomic diffusion is relatively slow and then the transitions between the odd-numbered planes can be open to competing mechanisms or at least additional mechanisms reducing the amount of

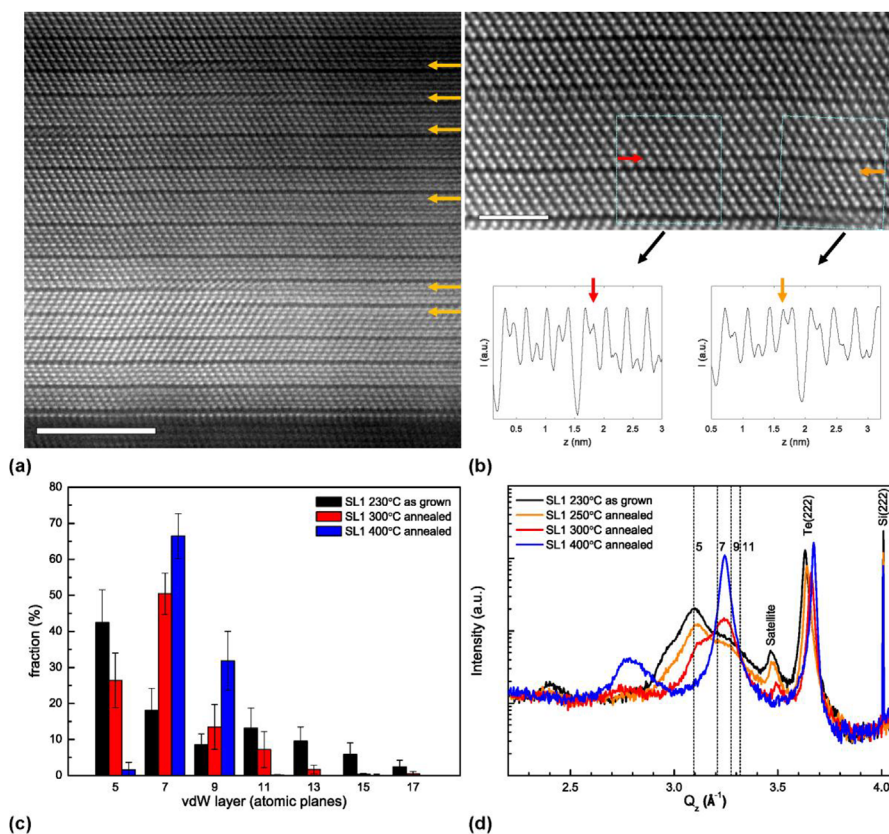


Figure 9. HAADF-STEM and XRD of a GeTe–Sb₂Te₃ CSL as grown by MBE at 230 °C and with subsequent annealing. a) Overview micrograph after 300 °C annealing. The orange arrows indicate the occurrence of bi-layer layer defects. Scale bar: 5 nm; b) close-up and intensity linescans of the bi-layer layer defects. The scans show that, directly after Te, Sb is most prevalent near the defects. Scale bar: 2 nm; c) distributions of 5-, . . . , 17-layered vdW blocks after different annealing temperatures as derived from the analysis of HAADF-STEM images; d) XRD symmetric ω -2 θ scans after different annealing temperatures. The Q_z positions for 5-, . . . , 11-layer ordering is indicated by vertical lines. Reproduced under the terms of a Creative Commons Attribution-NonCommercial 3.0 Unported Licence.^[50] Copyright 2017, The Royal Society of Chemistry.

long-range diffusion required. The abundant observation of the bilayer defects now suggest such a mechanism to switch between the odd-numbered blocks. Unfortunately the STEM images only provide a static snapshot and observing dynamics at this resolution is challenging, although not impossible. An experiment like this has been performed recently by in-situ heating (a thin electron transparent region of) Ge₆Sn₂Sb₂Te₁₁ at 280 °C in a TEM.^[53] These in situ TEM heating experiments showed that order in the stable phase is increased by in-plane movement of the bi-layer defects. The sizes of the domains with dissimilar sized building blocks were reduced in favor of the domains with similar sized building blocks.

Theory can also be a powerful tool to simulate the potential movement of the bilayer defects. Dynamical mechanisms by which the bilayer defects can slide were proposed in ref. ^[52] and the energetics of these mechanisms were calculated using density functional theory (DFT). The calculations indeed show that reasonable mechanism can be devised, where effectively the Sb atoms and Te atoms at the boundary line separating the two differently stacked region exchange their position and in the meantime shift from one vdW block across the vdW gap to the adjacent vdW block. This process might happen by a successive “snake-like” motion of the Sb and Te atoms along the boundary

line which require an activation energy that can be provided by thermal energy at 300 °C.^[52] Another interesting and arguable possibility is that a (Te or Sb) vacancy is present at the boundary line which then moves along this line as a “kink.” When vacancies are present the activation energies for bilayer defect movement is only about 0.5–0.7 eV, clearly lower than the about 1.7 eV provided by 300 °C thermal energy.

The presence of high vacancy concentrations in GST alloys is well-known for GST compounds. Particularly in the metastable rocksalt structure GST, vacancies on the Ge/Sb sublattice are necessary (with for instance 20% vacancies for GST225). One might argue that during the transition from the metastable to the stable GST structure these vacancies first gather themselves in vacancy layers after which these layers collapse into vdW gap and that therefore the vacancy concentration in stable GST is low. However, the same paper from which Figure 9 was extracted showed that the nominal composition of the analyzed films was close to GST124 and should thus be almost completely based on seven layered vdW layer blocks.^[50] However, a large fraction of 9 layered vdW layer blocks was observed in the 400 °C annealed sample (see Figure 9c). This discrepancy can be resolved when in the stable GST still an appreciable fraction of vacancies is present on Ge and Te sites, and since also the Sb-rich layer adjacent the

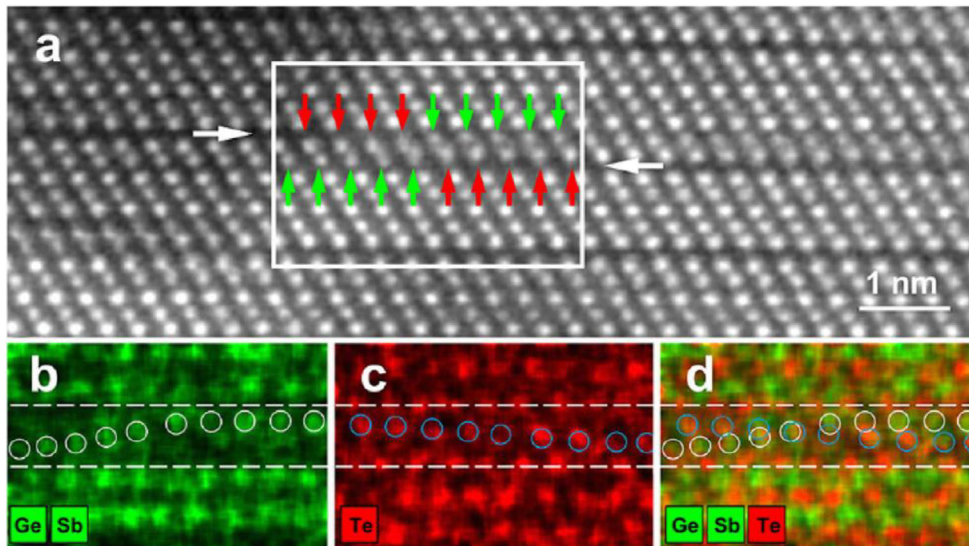


Figure 10. HAADF image and corresponding EDX map of a bilayer defect. a) HAADF image of bilayer defect. Green and red arrows mark the Sb-rich and Te-rich layer, respectively. b–d) Corresponding EDX mappings of the area inside the white box marked in (a). The centers of each Ge/Sb and Te atomic column are marked with white and blue circles, respectively. A smooth and continuous crossing of the Sb-rich and Te-rich layer is observed. The overlaid EDX mapping in (d) also indicates some intermixing of Sb and Te in the bilayers, which has been identified as an essential ingredient for the stability of the defects from DFT simulations. Reproduced with permission.^[51] Copyright 2018, American Chemical Society.

vdW gap can readily contain 1/3 of Ge sites, vacancies can also end up there.

This detailed attention to bilayer defects seems somewhat exaggerated, but becomes less odd when these defects can be associated with the switching behavior of the CSL memory. Suppose we start with GST225 with GeTe in the center of the vdW blocks and SbTe layers at the vdW gaps. When a SbTe bilayer defect shifts a vdW gap two layers up or down this might imply that we form locally GST236+GST214. Kolobov et al.^[54] calculated, using DFT simulations, that although the “Kooi phase” (GST225) essentially possesses a band gap (GGA is known to underestimate the band gap), the phase with the reconfigured vdW gap (2GST225 \Rightarrow GS T214 + GST236) clearly possesses a finite density of states at the Fermi level. This could be an explanation for the large resistivity contrast between the two phases despite them both being in a crystalline state. Kolobov et al. state that they do not associate the SET and RESET states directly with pure 2GST225 and (GST214 + GST236) phases, respectively. The only claim they want to make is that the proposed vdW gap reconfiguration may lead to dramatic changes in electronic properties.

This claim is in contradiction with the findings in a very recent paper where atomic scale elemental analysis using STEM-EDX is combined with DFT calculations;^[51] see the example image in Figure 10. In this paper the atomic models used for DFT simulations are made in closer agreement with the experimental observations than the models in ref.^[54], for instance with a cation sublattice on which Sb planes are nearest to the vdW gaps and Ge in the middle of the vdW blocks. Not only bilayer defects were analyzed by DFT calculations, but also other defects like twinning (across vdW gap), stacking disorder, and Ge/Sb compositional disorder on the cation sublattice. All these defects, according to the DFT calculations, do not affect the

metallic character of the compound. The only noticeable effect of the bilayer defects is that they can create localized states at the tail of the conduction band. This should not affect the metallic behavior at room and low temperatures, because the Fermi level lies at the top of the valence band. Potentially it can affect transport at elevated temperatures or high electrical fields, where massive electron excitations to the conduction band take place. Of course, defects in the trigonal GST like bilayer defects act as sources for electron scattering and thereby affect the electrical resistance, but it is rather unlikely that they can induce a metal-insulator transition. Given these two recent contradictory papers it is currently still an open question whether the bilayer defects have any direct relation with the switching between the two resistance states in the CSL memory. Nevertheless, for the dynamic reconfiguration of the GST compounds with trigonal structures these defects appear highly relevant.

2.4. An Outlook Including Alternative Switching Models

The focus of the present review paper is on TEM and STEM results acquired from CSL and the implication of these results for the SET and RESET states in the CSL memory. Still, many (potential) switching mechanisms for CSL memory have been proposed that are not rigorously based on experimentally obtained atomic resolution structure information, where particularly HAADF-STEM and STEM-EDX can be considered to date the most powerful techniques to derive this information. These switching mechanisms therefore in principle are outside the scope of the present review paper. Nevertheless, we will shortly discuss some of them, because they are also well-suited to finalize this review paper towards an outlook on possible next steps in the research of CSL with TEM-based techniques.

A potential switching mechanism could still involve a partial amorphization of the CSL that may occur locally at the interfaces or for one of the sublayer types. Particularly the now well-documented observation of the reconfiguration of the GeTe–Sb₂Te₃ superlattice into a GST–Sb₂Te₃ superlattice suggests that the thin GST sublayers might switch between the amorphous and crystalline states in between an Sb₂Te₃ scaffold that would remain (always) crystalline. This switching mechanism can explain that the resistance levels of the CSL memory remain rather similar to the ones of the ordinary GST memory cell, but that the presence of the many interfaces in the CSL leads to thermal confinement that may improve the energy efficiency related to switching the cell. Proof for this potential switching mechanism can in principle be obtained readily from TEM samples extracted from memory cells in the SET and even more importantly RESET states. For extraction of such TEM samples a FIB system is today the most logical solution. Like mentioned in section 2.1, making such FIB samples is not trivial, because during sample preparation samples might be damaged leading to further amorphization, but it is also possible that very thin amorphous layers (in-between crystalline layers) might recrystallize during the sample preparation. Fortunately, nowadays FIBs (or more often Dual Beam SEM-FIBs) are available allowing very gentle ion milling at low kV in the final milling steps. Nevertheless, still problems related to electrostatic discharge during FIB milling have to be avoided. This for instance requires that layers that would become isolated during the milling have to be connected first using a Pt conductive line to the larger Pt strip covering the original sample surface.^[55]

A totally different issue is that when presenting HAADF-STEM atomic structure results, which are directly related to the SET and RESET state of the CSL memory, a reader must receive sufficient supporting information such that there is confidence that the actual images shown are from the specific states and are produced by a method of which sufficient details are disclosed. Unfortunately such results have not been presented to date and therefore leave the question open what the actual atomic structures are in the SET and RESET states. Hence, answering this question based on careful TEM specimen extraction from the CSL memory cells in the SET and the RESET states can be considered the most important challenge for the present research field on CSL-memory.

There is extensive evidence that the structures in CSL may show rather exotic physics phenomena such as topological insulating (TI) behavior. One of the sublayers, Sb₂Te₃, is a well-known topological insulator.^[56,57] This also holds for specific types of atomic stacking in the trigonal GST structures (e.g., ref. ^[58]). GeTe can be considered a normal insulator. Still, in its ground state it experiences a kind of Peierls distortion ^[59] leading to weak ferroelectric order with polarization along the [111] axis of the rhombohedral lattice (which is the [0001] axis when hexagonal notation is used for the trigonal structure). Therefore the interfaces between Sb₂Te₃ and GeTe may show special behavior, where the conductive states at the interfaces may be switched on or off by electrical field or potentially also stress (pressure) (e.g., ref. ^[58]). The relation of the CSL with TI behavior has even resulted in a potential naming of the CSL memory as topological-switching random access memory TRAM.^[60]

However, it is highly doubtful if the SET and RESET states are dictated by TI behavior. The reason is that well-known TI

materials, such as Sb₂Te₃ or materials with similar structure (like Bi₂Se₃ and Bi₂Te₃ or their combinations), when grown in thin films generally contain many defect obscuring TI behavior in transport measurements.^[61] TI behavior can be detected by angle-resolved photo-emission spectroscopy, but the difference between the bulk insulating phase and the surface conducting state is obscured by bulk conductivity via defects. A related issue holds for GeTe that generally contains a relatively large concentration of vacancies on the Ge sublattice and thereby becomes a degenerate p-type semiconductor by self-doping (the Fermi level is localized in the top of the valence band). Probably the only role TEM or STEM can play in detecting TI behavior is that with these techniques the precise atomic stacking of the structures can be imaged and then the derived atomic models can be input for ab-initio calculations that predict whether TI behavior is present or absent.

Finally, also strain can have a significant effect on the switching mechanism in CSL memory. These superlattices are strongly dominated by vdW gaps in the out-of-plane stacking direction. At first sight it is not expected that strain can play a role in such structures, because strain would immediately relax at the vdW gap. At least this is underlying the popular view of the Nobel prize laureates Novolosoov and Geim that one can readily produce all kinds of heterostructures by stacking different types of 2D materials on top of each other.^[62,63] However, recent works have shown conclusively that strain plays a role in heterostructures based on combining two of the following three materials: Sb₂Te₃, Bi₂Te₃, and GeTe.^[64,65] Potentially the well-known 2D materials like graphene, BN and transition metal dichalcogenides cannot cause such mutual strains, suggesting a different type of vdW gap bonding between them than holds in case of Sb₂Te₃ and Bi₂Te₃.^[65]

Still, the presence of strain does not have to imply that strain will be important for the switching in the CSL memory. However, several recent papers from the group of Simpson advocate the importance of strain for the switching.^[17,18,66] Their work often rely on a combination of ab-initio (DFT or molecular dynamics) simulations and experiments. Their analyses show that particularly the strain experienced by the GeTe sublayer remarkably affects the switching. They vary the strain in GeTe by varying the Sb₂Te₃ thickness: For a CSL with 4 nm Sb₂Te₃ and 1 nm GeTe the strain in the GeTe is 2.2%, for a 2 nm Sb₂Te₃ and 1 nm GeTe it is 1.4%, for a 1 nm Sb₂Te₃ and 1 nm GeTe it is 0.4%. Increasing in this way the Sb₂Te₃ thickness significantly reduces the threshold voltage, switching time and RESET current of the Sb₂Te₃–GeTe CSL devices. Moreover, the biaxial tensile strain applied to the GeTe layer remarkably extended the switching endurance of the CSL devices due to less energy being used to switch the devices. This greatly improved switching performance of the CSL devices is attributed to the strained GeTe 2D premelt disordering within the Sb₂Te₃ scaffold.^[18]

Remarkable about these papers of Simpson et al. is that it is not explained properly how strain is determined experimentally. In the initial paper^[17] it is stated that the in-plane strain is determined based on the experimentally obtained *a* lattice parameter from Rietveld refined XRD patterns. However, these XRD patterns only show (0001) reflections, which is logical because the patterns are taken in $\theta/2\theta$ geometry of highly textured films with the c-axis out of the plane. Hence, only

information on the c lattice parameter can be obtained in this way and not the a lattice parameter. Therefore, it is not clear how strain is determined. Then, the follow up papers^[18,66] refer back to this initial paper concerning how strain is quantified and thus also not clarify the issue. The ab-initio calculations are based on models with pure Ge-Te planes adjacent to the vdW gap (i.e., –Ge–Te–vdWgap–Te–Ge–), whereas it seems that it is now well-established that these pure Ge planes must be replaced by Sb-rich planes. The relevance of such ab-initio calculations for experimental observations can therefore be doubted. At any rate, it exemplifies that to date we have not been able to reach sufficient consensus regarding the structures that occur in GeTe-Sb₂Te₃ superlattices.

3. Concluding Remarks

The evidence of an about order of magnitude power reduction in CSL compared to ordinary PCM has been clearly verified by several independent groups. However, it is not yet resolved what physical mechanism causes this reduction. All current mechanisms explaining the switching behavior of CSL memory are of speculative nature and evidence for a certain mechanism are till date actually absent or at least very poor. To obtain convincing proofs, there is little doubt that TEM-based techniques will play a crucial role to pinpoint the structures that occur in the SET and RESET states.

It is currently also unclear what the success rate is of producing CSL memory with superior performance. For scientific purposes it is sufficient to have a few working devices (when many fail), but in order to have a successful technology, the bit error rate should be extremely low. It is highly questionable whether CSL memory can become a sufficiently robust technology to meet the semiconductor standards with very low tolerances and precise requirements on many aspects. Moreover, even when the initial CSL memory cells might work well, it is not guaranteed that the CSL will stay intact during prolonged switching, e.g. the bit might be melt-quenched, ending up behaving like a regular GST memory cell. Results on endurance tests have been presented (with one example already shown in the seminal paper of Simpson et al.,^[16] but also more recently^[65]) showing favorable performance of the CSL memory compared to ordinary GST memory. Still, this holds for single cells and it has to be verified whether it can be transferred to all bits in a full memory. Experimental verification of the data retention of CSL memory is even a more open issue, because a (single) precise assessment seems to be lacking.

Despite these factors that might hamper implementation of CSL as an actual memory device, the CSL appears to be a very rich playground for producing new artificial structures with a potential wealth of interesting properties and solid-state physics phenomena. For instance, in the present work the focus has been on CSL memory that is purely associated with electrical properties, but CSLs can also be of interest for their thermoelectric, optical, optoelectronic, magneto-optical and magneto-electrical properties and for the field of meta-materials. Therefore, for many years to come there appears to be a bright future for CSL research with great prospects for innovative research.

Acknowledgements

This work was supported by the EU within the FP7 project PASTRY (GA 317746).

Conflict of Interest

The authors declare no conflict of interest.

Keywords

chalcogenide superlattices, crystal structure, phase change memory, transmission electron microscopy, van der Waals gap

Received: October 23, 2018
Revised: December 17, 2018
Published online: January 28, 2019

- [1] Nature editorial, *Nat. News* **2015**, 520, 408.
- [2] M. M. Waldrop, *Nat. News* **2016**, 530, 144.
- [3] S. R. Ovshinsky, *Phys. Rev. Lett.* **1968**, 21, 1450.
- [4] M. Wuttig, N. Yamada, *Nat. Mater.* **2007**, 6, 824.
- [5] G. W. Burr, M. J. Breitwisch, M. Franceschini, D. Garetto, K. Gopalakrishnan, B. Jackson, B. Kurdi, C. Lam, L. A. Lastras, A. Padilla, B. Rajendran, S. Raoux, R. S. Shenoy, *J. Vac. Sci. Technol. B* **2010**, 28, 223.
- [6] W. H. P. Pernice, H. Bhaskaran, *Appl. Phys. Lett.* **2012**, 101, 171101.
- [7] C. Ríos, M. Stegmaier, P. Hosseini, D. Wang, T. Scherer, C. D. Wright, H. Bhaskaran, W. H. P. Pernice, *Nat. Photonics* **2015**, 9, 725.
- [8] P. Hosseini, C. D. Wright, H. Bhaskaran, *Nature* **2014**, 511, 206.
- [9] C. Ríos, P. Hosseini, R. A. Taylor, H. Bhaskaran, *Adv. Mater.* **2016**, 28, 4720.
- [10] G. W. Burr, R. M. Shelby, A. Sebastian, S. Kim, S. Kim, S. Sidler, K. Virwani, M. Ishii, P. Narayanan, A. Fumarola, L. L. Sanches, I. Boybat, M. L. Gallo, K. Moon, J. Woo, H. Hwang, Y. Leblebici, *Adv. Phys. X* **2017**, 2, 89.
- [11] T. Tuma, A. Pantazi, M. L. Gallo, A. Sebastian, E. Eleftheriou, *Nat. Nanotechnol.* **2016**, 11, 693.
- [12] M. Boniardi, A. Redaelli, C. Cupeta, F. Pellizzer, L. Crespi, G. D'Arrigo, A. L. Lacaita, G. Servalli, in *2014 IEEE Int. Electron Devices Meet. (IEDM)*, IEEE Xplore **2014**, pp. 29.1.1–29.1.4.
- [13] S.-H. Lee, Y. Jung, R. Agarwal, *Nat. Nanotechnol.* **2007**, 2, 626.
- [14] M. Salinga, B. Kersting, I. Ronneberger, V. P. Jonnalagadda, X. T. Vu, M. L. Gallo, I. Giannopoulos, O. Cojocaru-Miréidin, R. Mazzarello, A. Sebastian, *Nat. Mater.* **2018**, 17, 681.
- [15] F. Xiong, A. D. Liao, D. Estrada, E. Pop, *Science* **2011**, 332, 568.
- [16] R. E. Simpson, P. Fons, A. V. Kolobov, T. Fukaya, M. Krbal, T. Yagi, J. Tominaga, *Nat. Nanotechnol.* **2011**, 6, 501.
- [17] X. Zhou, J. Kalikka, X. Ji, L. Wu, Z. Song, R. E. Simpson, *Adv. Mater.* **2016**, 28, 3007.
- [18] J. Kalikka, X. Zhou, E. Dilcher, S. Wall, J. Li, R. E. Simpson, *Nat. Commun.* **2016**, 7, 11983.
- [19] J. Tominaga, R. E. Simpson, P. Fons, A. V. Kolobov, *Appl. Phys. Lett.* **2011**, 99, 152105.
- [20] J. Tominaga, Y. Saito, K. Mitrofanov, N. Inoue, P. Fons, A. V. Kolobov, H. Nakamura, N. Miyata, *Adv. Funct. Mater.* **2017**, 27, 1702243.
- [21] K. Shportko, S. Kremers, M. Woda, D. Lencer, J. Robertson, M. Wuttig, *Nat. Mater.* **2008**, 7, 653.
- [22] A. V. Kolobov, P. Fons, J. Tominaga, *Sci. Rep.* **2015**, 5, 13698.

- [23] M. Zhu, O. Cojocaru-Mirédin, A. M. Mio, J. Keutgen, M. Küpers, Y. Yu, J.-Y. Cho, R. Dronskowski, M. Wuttig, *Adv. Mater.* **2018**, *30*, 1706735.
- [24] A. V. Kolobov, P. Fons, A. I. Frenkel, A. L. Ankudinov, J. Tominaga, T. Uruga, *Nat. Mater.* **2004**, *3*, 703.
- [25] J. Tominaga, P. Fons, A. Kolobov, T. Shima, T. C. Chong, R. Zhao, H. K. Lee, L. Shi, *Jpn. J. Appl. Phys.* **2008**, *47*, 5763.
- [26] E. G. T. Bosch, I. Lazić, *Ultramicroscopy* **2015**, *156*, 59.
- [27] J. Tominaga, A. V. Kolobov, P. Fons, T. Nakano, S. Murakami, *Adv. Mater. Interfaces* **2014**, *1*, 1300027.
- [28] D. Bang, H. Awano, J. Tominaga, A. V. Kolobov, P. Fons, Y. Saito, K. Makino, T. Nakano, M. Hase, Y. Takagaki, A. Giussani, R. Calarco, S. Murakami, *Sci. Rep.* **2014**, *4*, 5727.
- [29] J. Tominaga, A. V. Kolobov, P. J. Fons, X. Wang, Y. Saito, T. Nakano, M. Hase, S. Murakami, J. Herfort, Y. Takagaki, *Sci. Technol. Adv. Mater.* **2015**, *16*, 014402.
- [30] Y. Saito, J. Tominaga, P. Fons, A. V. Kolobov, T. Nakano, *Phys. Status Solidi RRL – Rapid Res. Lett.* **2014**, *8*, 302.
- [31] M. Küpers, P. M. Konze, S. Maintz, S. Steinberg, A. M. Mio, O. Cojocaru-Mirédin, M. Zhu, M. Müller, M. Luysberg, J. Mayer, M. Wuttig, R. Dronskowski, *Angew. Chem. Int. Ed.* **2017**, *52*, 10204.
- [32] N. Takaura, T. Ohyanagi, M. Tai, M. Kinoshita, K. Akita, T. Morikawa, H. Shirakawa, M. Araidai, K. Shiraishi, Y. Saito, J. Tominaga, in *2014 IEEE Int. Electron Devices Meet. (IEDM)*, IEEE Xplore **2014**, pp. 29.2.1–29.2.4.
- [33] N. Yamada, T. Matsunaga, *J. Appl. Phys.* **2000**, *88*, 7020.
- [34] S. Soeya, T. Shintani, T. Odaka, R. Kondou, J. Tominaga, *Appl. Phys. Lett.* **2013**, *103*, 053103.
- [35] T. Ohyanagi, N. Takaura, M. Tai, M. Kitamura, M. Kinoshita, K. Akita, T. Morikawa, S. Kato, M. Araidai, K. Kamiya, T. Yamamoto, K. Shiraishi, in *2013 IEEE Int. Electron Devices Meet. (IEDM)*, IEEE Xplore **2013**, pp. 30.5.1–30.5.4.
- [36] T. Ohyanagi, N. Takaura, M. Kitamura, M. Tai, M. Kinoshita, K. Akita, T. Morikawa, J. Tominaga, *Jpn. J. Appl. Phys.* **2013**, *52*, 05FF01.
- [37] M. Tai, T. Ohyanagi, M. Kinoshita, T. Morikawa, K. Akita, M. Takato, H. Shirakawa, M. Araidai, K. Shiraishi, N. Takaura, *2015 Symp. VLSI Technol.*, IEEE Xplore **2015**, pp. T96–T97.
- [38] T. Ohyanagi, M. Kitamura, M. Araidai, S. Kato, N. Takaura, K. Shiraishi, *Appl. Phys. Lett.* **2014**, *104*, 252106.
- [39] X. Yu, J. Robertson, *Sci. Rep.* **2015**, *5*, 12612.
- [40] J. Momand, R. Wang, J. E. Boschker, M. A. Verheijen, R. Calarco, B. J. Kooi, *Nanoscale* **2015**, *7*, 19136.
- [41] T. Matsunaga, N. Yamada, *Phys. Rev. B* **2004**, *69*, 104111.
- [42] T. Matsunaga, N. Yamada, Y. Kubota, *Acta Crystallogr. B* **2004**, *60*, 685.
- [43] T. Matsunaga, R. Kojima, N. Yamada, K. Kifune, Y. Kubota, M. Takata, *Appl. Phys. Lett.* **2007**, *90*, 161919.
- [44] P. Urban, M. N. Schneider, L. Erra, S. Welzmler, F. Fahrnbauer, O. Oeckler, *CrystEngComm* **2013**, *15*, 4823.
- [45] R. Wang, V. Bragaglia, J. E. Boschker, R. Calarco, *Cryst. Growth Des.* **2016**, *16*, 3596.
- [46] J. Momand, F. R. L. Lange, R. Wang, J. E. Boschker, M. A. Verheijen, R. Calarco, M. Wuttig, B. J. Kooi, *J. Mater. Res.* **2016**, *31*, 3115.
- [47] A. Lotnyk, I. Hilmi, U. Ross, B. Rauschenbach, *Nano Res.* **2018**, *11*, 1676.
- [48] P. Kowalczyk, F. Hippert, N. Bernier, C. Mocuta, C. Sabbione, W. Batista-Pessoa, P. Noé, *Small* **2018**, *14*, 1704514.
- [49] U. Ross, A. Lotnyk, E. Thelander, B. Rauschenbach, *J. Alloys Compd.* **2016**, *676*, 582.
- [50] J. Momand, R. Wang, J. E. Boschker, M. A. Verheijen, R. Calarco, B. J. Kooi, *Nanoscale* **2017**, *9*, 8774.
- [51] J.-J. Wang, J. Wang, H. Du, L. Lu, P. C. Schmitz, J. Reindl, A. M. Mio, C.-L. Jia, E. Ma, R. Mazzarello, M. Wuttig, W. Zhang, *Chem. Mater.* **2018**, *30*, 4770.
- [52] X. Yu, J. Robertson, *Sci. Rep.* **2016**, *6*, 37325.
- [53] C. Koch, T. Dankwort, A.-L. Hansen, M. Esters, D. Häubler, H. Volker, A. von Hoegen, M. Wuttig, D. C. Johnson, W. Bensch, L. Kienle, *Acta Mater.* **2018**, *152*, 278.
- [54] A. V. Kolobov, P. Fons, Y. Saito, J. Tominaga, *ACS Omega* **2017**, *2*, 6223.
- [55] B. J. Kooi, J. L. M. Oosthoek, M. A. Verheijen, M. Kaiser, F. J. Jedema, D. J. Gravesteijn, *Phys. Status Solidi B* **2012**, *249*, 1972.
- [56] H. Zhang, C.-X. Liu, X.-L. Qi, X. Dai, Z. Fang, S.-C. Zhang, *Nat. Phys.* **2009**, *5*, 438.
- [57] Y. L. Chen, J. G. Analytis, J.-H. Chu, Z. K. Liu, S.-K. Mo, X. L. Qi, H. J. Zhang, D. H. Lu, X. Dai, Z. Fang, S. C. Zhang, I. R. Fisher, Z. Hussain, Z.-X. Shen, *Science* **2009**, *325*, 178.
- [58] J. Kim, J. Kim, S.-H. Jhi, *Phys. Rev. B* **2010**, *82*, 201312.
- [59] D. Lencer, M. Salinga, M. Wuttig, *Adv. Mater.* **2011**, *23*.
- [60] N. Takaura, T. Ohyanagi, M. Tai, T. Morikawa, M. Kinoshita, K. Akita, in *2014 14th Annu. Non-Volatile Mem. Technol. Symp. (NVMTS)*, IEEE Xplore **2015**. <https://doi.org/10.1109/NVMTS.2014.7060835>.
- [61] N. Bansal, Y. S. Kim, M. Brahlek, E. Edrey, S. Oh, *Phys. Rev. Lett.* **2012**, *109*, 116804.
- [62] A. K. Geim, I. V. Grigorieva, *Nature* **2013**, *499*, 419.
- [63] K. S. Novoselov, A. Mishchenko, A. Carvalho, A. H. C. Neto, *Science* **2016**, *353*, aac9439.
- [64] P. A. Vermeulen, J. Mulder, J. Momand, B. J. Kooi, *Nanoscale* **2018**, *10*, 1474.
- [65] R. Wang, F. R. L. Lange, S. Cecchi, M. Hanke, M. Wuttig, R. Calarco, *Adv. Funct. Mater.* **2018**, *28*, 1705901.
- [66] X. Zhou, J. K. Behera, S. Lv, L. Wu, Z. Song, R. E. Simpson, *Nano Futures* **2017**, *1*, 025003.